Variations in N_{cn} and N_{ccn} over China marginal seas related to marine traffic

emissions, new particle formation and aerosol aging

Yang Gao[1,2#*], Deqiang Zhang[1#], Juntao Wang[1], Huiwang Gao[1,2] and Xiaohong Yao[1,2*]

[1]Frontiers Science Center for Deep Ocean Multispheres and Earth System, and Key Laboratory of Marine Environment and Ecology, Ministry of Education, Ocean University of China, Qingdao, 266100, China

[2]Laboratory for Marine Ecology and Environmental Science, Qingdao National Laboratory for Marine Science and Technology, Qingdao, 266237, China

[#]Authors contribute equally to this study

[*]Correspondence to yanggao@ouc.edu.cn; xhyao@ouc.edu.cn

Abstract

In this study, a cruise campaign was conducted over China marginal seas to measure concentrations of condensation nuclei (N_{cn}), cloud condensation nuclei (N_{ccn}) and other pollutants during DOY 110 to DOY 135 of 2018. With exhaustedly excluded self-ship emission signals, the mean values of N_{ccn} during the cruise campaign slightly increased from $3.2 \pm 1.1 \times 10^3$ cm^{-3} (mean $\pm$ standard) at supersaturation (SS) of 0.2% to $3.9 \pm 1.4 \times 10^3$ cm^{-3} at SS of 1.0%, and the mean value for N_{cn} was $8.1 \pm 4.4 \times 10^3$ cm^{-3}. Data analysis showed that marine traffic emissions apparently yielded a large contribution to the increase of N_{cn} in daytime, especially in marine atmospheres over their heavily travelled sea zones; however, the fresh sources had no clear contribution to the increase of N_{ccn}. This finding was supported by the quantitative relations between N_{cn} and N_{ccn} at SS=0.2-1.0% against mixing ratios of SO_2 in self-ship emission plumes, i.e., 1 ppb increase in SO_2 corresponds to 1.4×10^4 cm^{-3} increase in N_{cn}, but only 30-170 cm^{-3} increase in N_{ccn} possibly because of abundant organics in the aerosols. The smooth growth of marine traffic derived particles can be observed, reflecting aerosol aging. The estimated hygroscopicity parameter (κ) values were generally as high as 0.46-0.55 under the dominant onshore winds, suggesting inorganic ammonium aerosols likely acting as the major contributor to N_{ccn} through aerosol aging processes largely decomposed organics. Moreover, the influences of the transported new particles from the continent on N_{cn} and N_{ccn} in the marine atmosphere were also investigated.

Key words: N_{cn}; N_{ccn}; marine traffic emissions; hygroscopicity parameter; SO_2

1. Introduction

Oceans occupy approximately 2/3 of the Earth's surface and water evaporation from oceans acts as the major source of moisture in the atmosphere. Aerosol-cloud interactions in marine atmospheres, covering from tropics to polar regions, thereby attract great attentions in the past few decades due to their impact on the climate change (Huebert et al., 2003; Yu and Luo, 2009; Quinn and Bates, 2011; Wang et al., 2014; Brooks and Thornton, 2018; Rosenfeld et al., 2019). However, large uncertainties still exist in various marine atmospheres, e.g., the sources of aerosols, concentrations of bulk cloud condensation nuclei (CCN) and aerosol CCN activation under various of supersaturation, etc. (Clarke et al., 2006; Decesari et al., 2011; Quinn and Bates, 2011; Saliba et al., 2019; Rosenfeld et al., 2019). The uncertainties are mainly determined by limited observations in marine atmospheres, although a few additional observations of number concentrations of aerosol (N_{cn}) and CCN (N_{ccn}) were recently reported in different marine atmospheres, e.g., over Mediterranean (Bougiatioti et al., 2009), Sea of Japan (Yamashita et al., 2011), Bay of Bengal (Ramana and Devi, 2016), coast of California (Ruehl et al., 2009) and the Northwest Pacific Ocean (Wang et al., 2019), etc.

Besides sea-spray aerosols and secondarily formed aerosols from sea-derived gaseous precursors (O'Dowd et al., 1997; Clarke et al., 2006; Quinn and Bates, 2011; Blot et al., 2013; Fossum et al., 2018), marine traffics also emit a large amount of aerosols and reactive gases (Chen et al., 2017). These pollutants may also directly or indirectly contribute to CCN therein, to some extent (Langley et al., 2010). In addition, the long-range transport of continental aerosols widely reportedly acted as an important source of CCN in marine atmospheres (Charlson et al., 1987; Huebert et al., 2003; Fu et al., 2017; Royalty et al., 2017; Sato and Suzuki, 2019; Wang et al., 2019). The continent-derived aerosol particles observed in marine atmospheres usually mix with different sources such as biomass burning, dust and anthropogenic emissions (Feng et al., 2017; Lin et al., 2015; Guo et al., 2014; Guo et al., 2016). An appreciable fraction of organics

3

reportedly exists in marine aerosols and continental aerosols upwind of oceans (O'Dowd et al., 2004; Feng et al., 2012; Quinn et al., 2015; Feng et al., 2016; Song et al., 2018; Ding et al., 2019). However, ammonium sulfate aerosols have been frequently reported to dominantly contribute to CCN-related aerosols in many marine atmospheres and lead to hygroscopicity parameter (κ) larger than 0.5 (Mochida et al., 2010; Cai et al., 2017; Fu et al., 2017; Royalty et al., 2017; Phillips et al., 2018). A question is automatically raised, i.e., where do particulate organics go in the marine aerosols enriched in ammonium sulfate? Anthropogenic emission such as SO_2, NO_x in general increase since 1980s, until recently started to decrease, i.e., SO_2 start to decrease from 2006 (Li et al., 2017) whereas NOx started to decrease since 2011 (Li et al., 2017; Liu et al., 2016). Together with the influence of the Asian Monsoon, the marginal seas of China are, therefore, inevitably affected by the outflow of continental aerosols (Guo et al., 2016; Feng et al., 2017). Observations of N_{cn} and N_{ccn} in marine atmospheres over China marginal seas helps to resolve the data scarcity, understand their sources and dynamic changes and better service the study of their potential climate impacts.

In this study, cruise campaigns were conducted to measure the N_{ccn}, N_{cn}, particle number size distributions, gaseous pollutants and aerosol composition of water-soluble ionic species over the marginal seas from 20 April 2018 (day of year (DOY) 110) to 15 May 2018 (DOY 135), traveling from the East China sea to the South China sea, and returning to the Yellow sea. Spatiotemporal variations in N_{cn}, N_{ccn} and CCN activities of aerosol particles were studied. The *Kappa* values of aerosol particles from DOY 110 to DOY 118 over the marine were calculated and analyzed. Finally, we tried to establish the correlations of N_{cn} and N_{ccn} with mixing ratios of SO_2 in self-ship plumes and ambient marine air. The correlation equations are valuable for the estimation of N_{cn} and N_{ccn} from SO_2 when the direct observations of N_{cn} and N_{ccn} are not available.

2. Experimental design

2.1 Instruments and data sources

119 A cruise campaign was conducted across China marginal seas from DOY 110 to DOY

120 135 of 2018 (Fig. 1a,b). A suite of instruments including a Fast Mobility Particle Sizer

121 (FMPS, TSI Model 3091), CCN counter (CCNC, DMT Model 100), Condensation

122 Particle Counter (CPC, TSI Model 3775), gas analyzers, Ambient Ion Monitor-Ion

123 chromatography (AIM-IC) etc., were onboard a commercial cargo ship *Anqiang 87* for

124 measurements. The FMPS was used to measure particle number size distributions with

125 mobility diameters from 5.6 nm to 560 nm in 32 channels at 1-second temporal

126 resolution with an inlet flow of 10 L min^{-1}. The CPC was used to report the N_{cn} ranging

127 from 4 nm (50% efficiency) to 3000 nm (N_{cn}) in 2-second time resolution with an inlet

128 flow of 1.5 L min^{-1}. The N_{cn} was then used to calibrate the particle number size

129 distributions simultaneously measured by the FMPS, on basis of the procedure

130 proposed by Zimmerman et al. (2015). Due to the severe oceanic condition and humid

131 weather conditions, the FMPS and CPC were out of service after DOY 118 and DOY

132 122, respectively. Prior to the campaign, the CCNC was calibrated with ammonium

133 sulfate particles based on the standard procedure detailed at Rose et al. (2008). The

134 calibration curve was shown in Fig. S1. The total flow rate of CCNC was 0.45 L min^{-1},

135 with a ratio of sample to sheath at 1/10, and five super saturations (SS) conditions were

136 selected including 0.2 %, 0.4 %, 0.6 %, 0.8 %, and 1.0 %. More detailed information

137 about the measurement of N_{ccn} can be found in Wang et al. (2019).

138

139 During the experiment, ambient particles were first sampled through a conductive tube

140 (TSI, US) and a diffusion dryer filled with silica gel (TSI, US), and then splitted into

141 different instruments with a splitter. All instruments were placed in an air-conditioned

142 container on the deck of ship, with inlet height of approximately 6 m above the sea

143 level. Regarding the gas analyzers, the ambient O_3 (Model 49i, Thermo Environmental

144 Instrument Inc., USA C-series), SO_2 (Model 43i, Thermo Environmental Instrument

145 Inc., USA C-series), and NO_x (Model 42i, Thermo Environmental Instrument Inc., USA

146 C-series) were measured in mixing ratios with temporal resolution of one-minute. The

147 CCNC and gas analyzers were operated properly throughout the entire campaign. The

148 same was true for AIM-IC, which was used to measure water-soluble ionic species in

149   ambient particles less than 2.5 μm.

150

151   In this study, the Hybrid Single-Particle Lagrangian Integrated Trajectory (HYSPLIT)

152   model from the NOAA Air Resources Laboratory was used to track the particle sources.

153   The input of HYSPLIT such as wind speed and wind direction was from the National

154   Center for Environmental Prediction (NCEP) Global Data Assimilation System (GDAS)

155   with spatial resolution of 0.5 degree.

156

157   The hygroscopicity parameter (κ) was calculated according to the method proposed by

158   Petters and Kreidenweis (2007).

159
$$\kappa = \frac{4A^3}{27D_d^3\ \ln^2 S_C}\ ,\ A = \frac{4\sigma_{s/a}\ M_w}{RT\rho_w}$$

160   where D_d is the dry diameter, S_C is the super saturation, M_w is the molecular weight

161   of water, $\sigma_{s/a}$, a constant of 0.072 J m^{-2}, represents the surface tension over the

162   interface of the solution and air, R is the universal gas constant, T is the ambient

163   temperature and ρ_w is the water density. The D_d was not measured directly and

164   assumed to be equal to the critical diameter for CCN activation (D_{crit}). D_{crit} was defined

165   as the particle diameter down to which by integrating from the largest diameter with

166   the number concentration equals to CCN concentration (Hung et al., 2014; Cheung et

167   al., 2020). The FMPS has a low size resolution, particularly at the size greater than 90

168   nm, which doesn't allow accurately calculating *Kappa* values at SS=0.2%. At SS=0.6%

169   and 0.8%, the *Kappa* value was not calculated considering the complication in the

170   explanation of the value, possibly reflecting the combined effects of particle size,

171   mixing state and chemical composition.

172

173   *2.2 Separating ambient signals of N_{cn} and N_{ccn} from self-ship emission*

174   The data measured during the cruise campaign were frequently interfered by self-ship

175   emission signals. The N_{cn} and N_{ccn} over the marginal seas were first distinguished based

176   on the source of ambient environment or self-ship emission. The data measured at

177   18:00-24:00 on DOY 115 were used to illustrate the separation (Fig. 2), with the size

178 distribution of particle number concentration during DOY 110-118 shown in Fig. S2-

179 S10 in the supporting information. At 18:00-21:11 LT (Local Time), the low N_{cn} of

180 $5.8\pm0.4 \times 10^3$ cm^{-3} were observed. The accumulation mode dominated in particle

181 number concentration with the median mobility mode diameter at 105±4 nm (Fig. 2a).

182 Afterwards, the N_{cn} rapidly increased by over one order of magnitude (Fig. 2b). The

183 dominant particle number concentration mode changed from accumulation mode to

184 Aitken mode, with the median mobility diameter of Aitken mode stabilized at 47±4 nm

185 in approximately 90% of the time. The rapid increase in N_{cn} and the change in mode

186 size indicated the signal of ship emission itself. The self-ship emission interference after

187 21:11 was also supported by additional evidences, e.g., a large decrease in activation

188 ratio (AR), defined as the quotient of N_{ccn} and N_{cn}, from >0.5 to <0.2 at SS=0.4% (Fig.

189 2c) due to large increase of N_{cn} but much smaller magnitude enhancement of N_{ccn} (Fig.

190 2b), a rapid increase of NO_x from <10 ppb to 192±99 ppb, NO/NO_2 from <0.1 to

191 0.7±0.3, as well as SO_2 from <2 ppb to 6.2±2.4 ppb. The large changes were expected

192 because the ship smoke stock was approximately only 10 meters away from these

193 detectors. Thus, based upon the feature described above certain criteria were designed

194 in this study to identify self-ship emission signals so as to separate from ambient signals,

195 i.e., a net increase in N_{cn} beyond 5×10^4 cm^{-3} in five minutes, the median mobility mode

196 diameter around 50 nm, NO_2>30 ppb and NO/NO_2>0.5.

197

198 **3. Results and discussion**

199 *3.1 Spatiotemporal variations in ambient N_{cn} during the cruise period*

200 Fig. 3 shows a time series of minutely averaged distributions of N_{cn}, N_{ccn} and AR at SS

201 of 0.4% and 1.0% from DOY 110 to DOY 135 2018, when self-ship emission signals

202 had been exhaustedly removed.

203

204 When spatiotemporal variations in N_{cn} were examined during the first half cruise period

205 (Fig. 3a), the N_{cn} spanned a broad range of 0.2-4.5$\times 10^4$ cm^{-3} with the average value

206 of 8.1 ± 4.4$\times 10^3$ cm^{-3}. Specifically, the N_{cn} were only 6.5 ± 0.8$\times 10^3$ cm^{-3} at 00:00-

207 06:00 LT on DOY110 when the ship anchored at the Yangtze River estuary near

208 Shanghai (Fig. 1). The low N_{cn} were comparable to the mean value of N_{cn} (5.4×10^3 cm$^-$

209 ^{3}) in marine-air cases during January-December 2010 in Shanghai reported by Leng et

210 al. (2013). The N_{cn} largely increased to $1.9 \pm 0.7 \times 10^4$ cm^{-3} at 08:00-21:00 LT on

211 DOY110 when the ship cruised across the Yangtze River estuary. The measured

212 particles in number concentration were dominantly distributed at Aitken mode on that

213 day while the median Aitken mode diameter shifted from 49±5 nm at 00:00-06:00 to

214 40±5 nm at 08:00-21:00 (Fig. S2). The Yangtze River estuary contains several world-

215 class ports and is heavily travelled by marine traffics in daytime (Chen et al., 2017).

216 Since the onshore wind dominated on that day (not shown), the increase in N_{cn} and the

217 decrease in median Aitken mode diameter at 08:00-21:00 LT possibly reflected the

218 increased contribution from marine traffic emissions. Marine traffics visibly decreased

219 when the ship left the Yangtze River estuary toward the south. The N_{cn} were then

220 significantly decreased, i.e., $9.5 \pm 4.4 \times 10^3$ cm^{-3} in the marine atmosphere over the sea

221 zone in Zhejiang Province (at 07:00 LT on DOY111 - 17:00 LT on DOY 114), with

222 P<0.01. The N_{cn} further decreased to the lower values of $5.8 \pm 1.7 \times 10^3$ cm^{-3} in the

223 marine atmosphere over the sea zone in Fujian Province (at 18:00 LT on DOY114 -

224 14:00 LT on DOY 117). All these values were, however, 1-2 orders of magnitude larger

225 than the background values in remote clear marine atmospheres, e.g., <300 particle cm$^-$

226 ^{3} without the influence of industrial activities in the western Pacific and the tropical

227 Pacific (Ueda et al., 2016) and those reported by Quinn and Bates (2011) and Saliba et

228 al. (2019), indicating overwhelming contributions from non-sea-spray aerosols

229 including marine traffic emissions, the long-range continental transport, newly formed

230 particles in marine atmospheres, etc. As reported, atmsopheric particles over China

231 marginal seas can be further transported to the remote northwest Pacific Ocean (NWPO)

232 in spring under westerly winds, e.g., N_{cn} observed over the NWPO in March-April 2014

233 were as high as $2.8 \pm 1.0 \times 10^3$ cm^{-3} and approxiately half of that over China marginal

234 seas observed in March 2014 (Wang et al., 2019).

235

236 The mean value of N_{cn} ($8.1 \pm 4.4 \times 10^3$) observed in this study was close to that of 7.6

237 $\pm 4.0 \times 10^3$ cm^{-3} (the number concentrations of particles larger than 10 nm) over the

238 eastern part of the Yellow sea in spring 2017 reported by Park et al. (2018). They

239 attributed the high number concentrations of particles within nucleation and Aitken

240 modes to the long-range transport of air pollutants over eastern China under the

influence of westerly winds. Consistently, larger values of N_{cn} were frequently observed in the continental atmospheres upwind of the Yellow sea, e.g., the mean values of $1.8 \pm 1.4 \times 10^4$ cm^{-3} in May 2013 in Qingdao, a coastal city in proximity to the Yellow Sea (Li et al., 2015), 3.18×10^4 cm^{-3} in February-August 2014 in Beijing (Dal Maso et al., 2016), and 1.0×10^4 cm^{-3} in continental-air cases during January-December 2010 in Shanghai (Leng et al., 2013).

3.2 Spatiotemporal variations in ambient N_{ccn} during the cruise period

N_{ccn} data were generally available during the entire campaign (Fig. 3b). The mean values of N_{ccn} over China marginal seas during the DOY 110 to DOY 135, 2018 were from $3.2 \pm 1.1 \times 10^3$ cm^{-3} to $3.9 \pm 1.4 \times 10^3$ cm^{-3} under SS ranging from 0.2% to 1.0%(Table 1), two to four times larger than the N_{ccn} at the same SS over the NWPO in March-April 2014 (Wang et al., 2019), and much higher, i.e., 1-2 orders of magnitude, than the pristine marine background values (Quinn and Bates, 2011). As was discussed in the previous section, the mean N_{cn} in this study ($8.1 \pm 4.4 \times 10^3$ cm^{-3}) was comparable to that of N_{cn} ($7.6 \pm 4.0 \times 10^3$ cm^{-3}) over the Yellow Sea in spring 2017 in Park et al. (2018); however, the comparison of mean N_{ccn} reveals that mean value ($3.6 \pm 1.2 \times 10^3$ cm^{-3}) at SS of 0.6% in this study was approximately 25% smaller than that (4.8×10^3 cm^{-3} at similar SS of 0.65%) in Park et al. (2018), likely a result of long range transport, considering the relatively distant (i.e., 500-600 km) observations away from the land depicted in Fig. 1 of Park et al., 2018, and the subsequently higher extent of aerosol aging. N_{ccn} under SS of 0.2% in this study ($3.2 \pm 1.1 \times 10^3$) is comparable to that ($3.1 \pm 1.9 \times 10^3$) by Li et al. (2015) in the continental atmosphere of Qingdao in May 2013, however, the increment of N_{ccn} with the increase of SS was much weaker in our study, resulting in on average of 36% smaller in N_{ccn} under SS of 0.4% to 1.0% compared to Li et al. (2015). Consistently, the sensitivity differences of N_{ccn} to SS between relatively clean (i.e., N_{cn} ($8.1 \pm 4.4 \times 10^3$) in this study) and polluted (with N_{cn} of $1.8 \pm 1.4 \times 10^4$ cm^{-3}) environment in Li et al. (2015) is also reported by Nair et al. (2019), who found little sensitivity of N_{ccn} to changes in SS over the equatorial Indian Ocean (< 6 °N) with relatively clean air, and much larger enhancement of N_{ccn} with the increase of SS in

271   polluted marine atmospheres (> 6 °N).

272

273   In addition, N_{ccn} at SS from 0.1% to 1.0% during the period with high NH_4^+ (17:00 LT

274   on DOY 114 to 10:00 LT on DOY 120) is statistically significant higher (P<0.01) in

275   comparison to the poor NH_4^+ period (11:00 LT on DOY 120 to 7:00LT on DOY 136;

276   Fig. 3b). More specifically, a large increase in NH_4^+ concentration, with mean

277   concentration of 6.3±2.5 μg m^{-3}, can be observed during the period from 17:00 LT on

278   DOY 114 to 10:00 LT on DOY 120 (Fig. 3b). The mean N_{ccn} during this period varied

279   from $3.5 \pm 1.0 \times 10^3$ cm^{-3} to $4.0 \pm 1.1 \times 10^3$ cm^{-3} at SS ranging of 0.2% to 1.0%. In contrast,

280   after DOY 120, the concentration of NH_4^+ (0.67±0.70 μg m^{-3}) substantially decreased

281   by almost 90%, during which the mean N_{ccn} at each SS showed statistically significant

282   decrease of 8% to 15%, implicative of the vital contribution to CCN of secondary

283   ammonium salt aerosols.

284

285   Another feature depicted in Fig. 3b is the N_{ccn} during the low NH_4^+ period may even

286   exceed the maximal value of N_{ccn} during the high NH_4^+ period. To elucidate the

287   underlying mechanism, the N_{ccn}, under each SS, was composited and compared

288   between the days with NH_4^+ concentration higher than the upper quartile and the days

289   in the lower quartile, yielding some interesting findings. At SS=0.2%, the composited

290   N_{ccn} under high NH_4^+ period was higher than that during low NH_4^+ period with

291   statistical significance level of 0.01. There was no significant difference in N_{ccn} between

292   the two composited periods at SS of 0.4% and 0.6%. However, the composited N_{ccn}

293   (i.e., only selection of the upper quartile) during the high NH_4^+ period was significantly

294   lower than the composited value during the low NH_4^+ period with P<0.01, e.g., $5.1 \pm$

295   0.5×10^3 cm^{-3} versus $5.3 \pm 0.7 \times 10^3$ cm^{-3} at SS=0.8%, $5.2 \pm 0.5 \times 10^3$ cm^{-3} versus $5.7 \pm$

296   0.7×10^3 cm^{-3} at SS =1.0%. During the low NH_4^+ period, the marine atmospheres over

297   the observational zones may sometimes receive strong continental inputs and/or marine

298   traffic emissions, leading to the larger N_{ccn}. Enhanced formation of ammonium salt

299   aerosols during the high NH_4^+ period likely canceled out or even overwhelmed

300   continental inputs and/or marine traffic emissions in increasing N_{ccn} at SS=0.2%.

In addition, fresh marine traffic emissions likely yielded a negligible contribution to N_{ccn} in the marine atmosphere because of a large amount of aged aerosols from various sources therein. For example, the mean values of N_{ccn} were 3.2×10^3 cm^{-3} and 4.5×10^3 cm^{-3} at SS=0.4% and 1.0% at 08:30-11:30 on DOY110, respectively. They were almost same as 3.2×10^3 cm^{-3} at SS=0.4% and 3.8×10^3 cm^{-3} at SS=1.0% before 06:00 on that day. The mean values of N_{cn}, however, largely increased from $6.5 \pm 0.8 \times 10^3$ cm^{-3} before 06:00 to $1.3 \pm 0.3 \times 10^4$ cm^{-3} at 08:30-11:30 when the ship cruised across the Yangtze River estuary (Fig. 3b).

3.3 Spatiotemporal variations in CCN activation and Kappa values

AR values at SS of 0.4% and 1.0% were examined in the section, shown in Fig. 3c. At SS=0.4%, AR values largely varied from 0.06 to 0.92 with the median value of 0.51. Specifically, AR values narrowly varied around 0.51 ± 0.04 at 00:00-06:00 LT on DOY110. At 08:00-21:00 LT on that day when the ship cruised across the Yangtze River estuary, the AR values were substantially decreased to 0.26 ± 0.06 concurrently with approximate 200% increase in N_{cn} values, i.e., N_{cn} value of $6.5 \pm 0.8 \times 10^3$ cm^{-3} at 00:00-06:00 LT and $2.0 \pm 0.7 \times 10^4$ cm^{-3} at 08:00-21:00 LT on DOY110 (Fig. 3a). The AR values then exhibited an oscillating increase from DOY 111 to DOY113. Low AR values of 0.12 ± 0.04 were suddenly observed at 10:00-18:00 LT on DOY114 in the presence of strong new particle signals transported from the upwind continental atmosphere, as discussed later. AR values, however, reached 0.34 ± 0.04 at 06:00-08:00 LT and 0.39 ± 0.08 at 19:00-24:00 LT on DOY114 with the new particle signals largely reduced. Even excluding the AR values on DOY 114, a significant difference was still obtained between AR values of 0.61 ± 0.12 during the high NH_4^+ period and those of 0.55 ± 0.17 during the low NH_4^+ period. Enhanced formation of ammonium salts seemingly increased CCN activity to some extent. At SS=1.0%, AR values showed large fluctuation with the median value of 0.57 ± 0.17 (Fig. 3c) and the temporal trend was similar to that at SS=0.4%.

To minimize the impact from particle sizes, *Kappa* values were further investigated. As was reported by Phillips et al. (2018), *Kappa* values in a high time resolution usually exhibited a broad distribution, reflecting the complexity due to various of factors. To reveal the key factors in determining *Kappa* values in a large spatiotemporal scale, the daily *Kappa* values of atmospheric aerosols were estimated, on basis of the daily mean N_{ccn} and the size distributions of particle number concentration from DOY 110-118 (Fig. 3c). Please note that for DOY 110, considering large differences of particle number concentration between 00:00-06:00 and 08:00-21:00 (Fig. S2), *Kappa* values were calculated separately for these two periods. At SS=0.4% (green dashed line in Fig. 3c), the estimated *Kappa* values were as high as 0.66 at 00:00-06:00 LT while it decreased to 0.37 at 08:00-21:00 LT on DOY110. The *Kappa* value varied narrowly from 0.46 to 0.55 on DOY 111-113, 115 and 117, implying that inorganic aerosols such as completely and incompletely neutralized ammonium salts may yield a large contribution to the N_{ccn}. These values were generally consistent with reported observations in most of marine atmospheres. For example, Cai et al. (2017) reported the *Kappa* value around 0.5 for particles with sizes of 40-200 nm at a marine site in Okinawa and sulfate to be the dominant component of aerosol particles on 1-9 November 2015, and a similar *Kappa* value in spring 2008 over this site was reported by Mochida et al. (2010). Royalty et al. (2017) reported *Kappa* values for 48, 96, and 144 nm dry particles to be 0.57 ± 0.12, 0.51 ± 0.09, and 0.52 ± 0.08 in the subtropical North Pacific Ocean and sulfate-like particles contributing at most 77–88% to the total aerosol number concentration. *Kappa* values over the Atlantic Ocean were observed around 0.54 ± 0.03 for 284 nm particles (Phillips et al., 2018).

The estimated *Kappa* values sometimes reached 0.66-0.67 (i.e., on DOY 116), which may be related to unidentified factors. For example, O'Dowd et al. (2014) proposed that some organics derived from sea-spray aerosols may also increase the N_{ccn}, to some extent, by reducing surface intension, leading to increase of *Kappa* values. A small fraction of sea-salt aerosols in submicron particles may also increase *Kappa* values since its *Kappa* value was as high as 1.3 (O'Dowd et al., 1997; O'Dowd et al., 2004).

The *Kappa* value of 0.29 was obtained on DOY118, close to *Kappa* values widely observed for continental atmospheric aerosols (~0.3) (Andreae and Rosenfeld, 2008; Poschl et al., 2009; Rose et al., 2010). The estimated *Kappa* value largely decreased to 0.15 on DOY114 when new particle formation (NPF) occurred, with detailed discussion in section 3.5. Moreover, at SS of 1.0%, the estimated *Kappa* value was always smaller than 0.2. The *Kappa* value of organics was commonly assumed as 0.1 (Rose et al., 2011; Cai et al., 2017; Singla et al., 2017). In general, the fraction of organics in nanometer particles increases with decreasing particle sizes (Rose et al., 2010; Rose et al., 2011; Crippa et al., 2014; Cai et al., 2017). A combination of the two factors likely led to overall *Kappa* values estimated at SS=1.0% to be much lower. However, the direct measurements of chemical composition of nanometer particles needed to confirm the arguments.

3.4 Particle number size distributions and CCN activation associated with marine traffic emissions and aerosol aging

The particle number size distributions during DOY 110-118, shown in Fig. 4, can be in general classified into two categories. Category 1 occurred on DOY110-114, when particle number concentrations were mainly distributed at the Aitken mode, whereas the accumulation mode was generally undetectable. Category 2 occurred on DOY115-118, when the accumulation mode can be clearly identified and generally dominated over the Aitken mode. Hoppel (1986) proposed cloud-modified aerosols to be mainly distributed at 80-150 nm in the remote tropical Atlantic and Pacific oceans. Cloud-modified aerosols are quite common in remote marine atmosphere, likely leading to the dominate accumulation mode particles to be observed on DOY115-118. Occasionally, the Aitken mode dominated over the accumulation mode on some day such as DOY 118. To further dive into the sources of different modes of particles, three-day of DOY112, DOY 116 and DOY118 were selected.

On DOY 112, the Aitken mode particles accounted for approximately 60% of the total

particle number concentration (Fig. 5a), with median Aitken mode diameters around 54±8 nm. Like the observations over the Yangtze River estuary, the mean value of N_{cn} increased by approximately 50% concurrently with a decrease in the median Aitken mode diameters by ~9 nm at 05:30 – 11:40 LT against those at the early morning before 05:30 LT (Fig. 5b). Concomitantly, the AR values decreased to 0.31±0.09 at SS of 0.4%, with similar AR decrease at SS of 1.0%, and the lowest AR and *Kappa* values occurring at 06:00-07:00 LT at SS of both 0.4% and 1.0%. All these results pointed towards the increase in Aitken mode particles at 05:30 – 11:40 LT to be likely derived from enhanced marine traffic contributions carried by the onshore wind from the south (Fig. S11). During other time on DOY112, the onshore wind may also carry the marine-traffic derived particles to the observational sea zones. However, the marine-traffic derived particles likely aged to some extent, e.g., the median Aitken mode diameters exhibited an oscillating increase from approximately 50 nm at 19:00 to approximately 70 nm at 24:00 LT with the particle growth rate of ~4 nm hour^{-1}. The AR values, however, narrowly varied around 0.47±0.03 at SS=0.4% and 0.52±0.05 at SS=1.0% during the particle growth period. The *Kappa* values at SS=0.4% gradually decreased from 0.56 at 19:00 to 0.41 at 23:00 LT, reflecting more aged marine-traffic derived particles growing into CCN size.

On DOY 116, the accumulation mode particles instead of Aitken mode particles dominantly contributed to N_{cn} (Fig. 5d), under the marine air influence from the northeast (Fig. S13). The median accumulation mode diameters narrowly varied around 135±5 nm at 01:00-13:00 LT and 102±5 nm at 16:20-24:00 LT with the transition period in between (Fig. 5e). The AR and *Kappa* values, however, showed no statistically significant difference during the two periods at SS of 0.4% and 1.0%, implying that the size change in accumulation mode particles showed a negligible influence on the CCN activation. Hourly variations in AR and *Kappa* values may be associated with other factors, e.g., chemical composition, mixing state, etc. (Gunthe et al., 2011; Rose et al., 2011).

419 On DOY 118, under the influence of mixture from the marine and coastal areas from

420 the northeast (Fig. S14), the accumulation mode particles generally dominated the

421 contribution to N_{cn} while the reverse was true in some occasions (Fig. 5g,h). The median

422 accumulation mode diameters exhibited an oscillating increase from approximately 100

423 nm to 130 nm at 00:00-08:00 LT, narrowly varied around 133±5 nm at 08:00-13:00 LT,

424 and then exhibited an oscillating decrease down to approximately 100 nm at 20:00 LT.

425 The AR values and *Kappa* values at SS=0.4%, however, exhibited an inverted bell-

426 shape with the lowest values at 0.31 and 0.11 at 13:00. The decreases in AR values and

427 *Kappa* may be related to organic condensed on accumulation mode particles since the

428 median accumulation mode diameters were almost largest at 13:00. The number

429 concentration of Aitken mode particles evidently enhanced at 14:00-15:00, but the

430 influence on AR values and *Kappa* values at SS=0.4% was undetectable (Fig. 5i).

431

432 *3.5 The long-range transport of grown new particles on DOY 114*

433 No hour-long sharp increase in number concentration of nucleation mode particles (<

434 20 nm) was observed during the period from DOY 110 to DOY 118, except on DOY114

435 (Fig. 4). According to the conventional definition of NPF events (Kulmala et al., 2004;

436 Dal Maso et al., 2005), the occurrence frequency of NPF events was low in this study.

437 Unlike continental atmospheres where a high occurrence frequency of NPF events has

438 been observed globally in spring (Kulmala et al., 2004; Kerminen et al., 2018), a low

439 occurrence frequency reportedly occurred over the seas during the "Meiyu (plum-rain)

440 season" in spring because of frequent rainy, foggy or cloudy weather conditions (Zhu

441 et al., 2019). Lack of NPF events in the marine atmospheres implied N_{cn} and N_{ccn} to be

442 mainly contributed by primarily emitted aerosols and their aged products.

443 During the period of 10:00-18:00 LT on DOY 114, a large increase in number

444 concentrations of Aitken mode particles (Fig. 6a) likely reflected the long-range

445 transport of grown new particles from upwind continental atmospheres (Fig. S12). The

446 size distributions of particle number concentration showed a dominant Aitken mode at

447 10:00-18:00 LT, when spatiotemporal variations in N_{cn} and median Aitken mode

448 diameters exhibited bell-shape patterns (Fig. 6b). The median Aitken mode diameters

449 increased from 26 nm at 10:00 LT to 33 nm at 12:00-13:00 LT and then decreased to 20

450 nm prior to the signal disappearance likely reflecting the growth and shrinkage of the

451 Aitken mode particles (Yao et al., 2010; Zhu et al., 2019). The median Aitken mode

452 diameters were evidently smaller than the values, i.e., 40-50 nm for Aitken mode

453 particles, observed over the Yangtze River estuary on DOY 112 (Fig. 5a). Moreover,

454 the number concentrations of 20-40 nm particles increased by 5.8 times at 12:00-13:00

455 LT compared to the mean value at 06:00-09:00 LT while the total number

456 concentrations of particles greater than 90 nm increased by only 67%. These results

457 implied the largely increased number concentrations of Aitken mode particles with a

458 dynamic change in mode diameter observed at 10:00-18:00 LT unlikely to be caused

459 by primarily emitted and aged particles from marine traffic emissions or other

460 combustion sources. The observations of gaseous and particulate species, during the

461 same period, implied air masses to be well-aged and less polluted. For instance, the

462 measured hourly average mixing ratios of SO_2 was no larger than 1.2 ppb (Fig. 6c) and

463 the hourly average concentrations of NH_4^+ in $PM_{2.5}$ were smaller than 2 $\mu g\ m^{-3}$ (Fig.

464 3b). In addition, the concentrations of K^+ were below 0.3 $\mu g\ m^{-3}$, suggesting negligible

465 contributions from biomass burning (Fig. 6e).

466

467 Before 09:00 LT, a much weaker spike of nucleation mode particles was intermittently

468 observed (Fig. 6a). The weak and intermittent NPF seems to occur in the marine

469 atmospheres before 09:00 LT when no apparent growth of new particles was observed.

470 Possibly due to the transport from the continent (Fig. S12) and an increase in the

471 condensational sink around 10:00 am (Fig. 6a), the weak NPF signal gradually dropped

472 to a negligible level half an hour later, concomitant with a large increase in the number

473 concentrations of Aitken mode particles at 10:00-18:00 LT.

474

475 N_{ccn} at SS=0.4% increased from $1.2 \times 10^3\ cm^{-3}$ at 06:00-09:00 LT to the peak value of

476 $2.3 \times 10^3\ cm^{-3}$ at 12:00 LT, with increase of 92%, and N_{ccn} at SS=1.0% increased from

477   1.6×10^3 cm^{-3} to 4.0×10^3 cm^{-3}, with increase of 150% (Fig. 6d). The net increase in

478   N_{ccn} at SS=0.4% likely reflected the contribution from pre-existing particles since new

479   particles with the diameter less than 50 nm were unlikely activated as CCN at such low

480   SS (Li et al., 2015; Wu et al., 2016; Ma et al., 2016). The larger net increase in N_{ccn} at

481   SS=1.0% may reflect the contributions mixed from pre-existing particles and grown

482   new particles. The high SS can activate particles as CCN with diameters down to 40

483   nm (Dusek et al., 2006; Li et al., 2015). The invasion of grown new particles also led

484   to the AR values largely decreased from 0.3 to 0.1 at SS=0.4%, and from 0.4 to 0.2 at

485   SS=1.0% (Fig. 6e). After 18:00 LT, the AR values retuned to 0.3-0.4 at SS=0.4% and

486   0.4-0.6 at SS=1.0%. When the calculated *Kappa* values were examined (Fig. 6c), they

487   decreased from 0.4 to 0.1-0.2 at SS=0.4%. The value returned to 0.3 at 18:00-19:00 LT

488   (FMPS was temporarily malfunctioned after 19:20 LT). The *Kappa* values were below

489   0.2 at SS=1.0% on that day. The decreases in AR values and *Kappa* values at two SS

490   were likely caused by organic vapor condensed on preexisting particles and new

491   particles (Wu et al., 2016; Zhu et al., 2019).

492

493   *3.6 Correlations of N_{cn} and N_{ccn} with SO_2 in self-ship plumes and ambient air*

494   When self-ship emission signals were detected, the observational values included a

495   combination of contributions from self-ship emissions and ambient concentrations.

496   Although ambient N_{cn} was negligible in comparison with N_{cn} derived from self-ship

497   emissions, it was not the case for N_{ccn} and SO_2.   Based on the minutely data, the signal

498   was considered as vessel-self emission when both N_{cn} greater than 50,000 cm^{-3} and SO_2

499   greater than 5 ppb. The composited data was then used to derive the hourly average N_{cn},

500   N_{ccn} and SO_2, which was then subtracted by the ambient hourly mean value during the

501   preceding hour with relatively clean conditions (i.e., concentration of N_{cn} lower than

502   10,000 cm^{-3}, SO_2 lower than 2.5 ppb). Please note uncertainties exist in terms of the

503   criteria and separation between self-ship and ambient signals, however, minimal impact

504   is expected in the relationship examined below.

505

506   Fig. 7a showed correlations of N_{cn} and N_{ccn} with mixing ratio of SO_2 in self-ship plumes,

507   prefixed by Δ for N_{cn}, N_{ccn} and SO_2 to implicate the removal of ambient signals. A good

508   correlation of 0.66 for R^2 (P<0.01) was obtained and the slope indicates that N_{cn}

509   increase by 1.4×10^4 cm^{-3} for each ppb increase of SO_2 resulted from ship emission

510   (Fig. 7a). High emissions of N_{cn} were generally reported in engine exhausts with high

511   sulfur-content diesel to be used (Yao et al., 2005; Yao et al., 2007). In regard of N_{ccn} at

512   SS of 0.2% to 1.0% (Fig. 7b), it increases from 30 cm^{-3} to 170 cm^{-3} per 1 ppb increase

513   of SO_2, showing statistical significant correlation at 99th confidence level. The

514   contribution ratio of SO_2 to N_{ccn} is 0.002 (SS of 0.2%), 0.004(SS of 0.4%) and 0.012

515   (SS of 1.0%) to that of N_{cn}, in general consistent with the previous study by Ramana

516   and Devi (2016), in which a range of 0.0012–0.57 was observed for CCN at 0.4% in

517   Bay of Bengal during Aug 13–16, 2012.

518

519   The correlations of hourly averaged N_{cn} and N_{ccn} with SO_2 in ambient air were examined

520   and showed in Fig. 7c,d. The data was segmented into pieces based on SO_2 with interval

521   of 0.2 ppb. A good correlation between the averaged N_{cn} and SO_2 were obtained with

522   R^2 of 0.80 (P<0.01) and 1 ppb increase in SO_2 likely increased N_{cn} by 1.6×10^3 cm^{-3}

523   (Fig. 7c). The increase in N_{cn} with SO_2 may reflect the contribution from primary

524   emissions. An intercept was, however, as large as 3.9×10^3 cm^{-3}, likely representing the

525   contribution from well-aged aerosols.

526

527   Hourly averaged N_{ccn} at different SS generally increased with increase of ambient SO_2

528   (Fig. 7d). A good correlation between the averaged N_{ccn} and SO_2 were obtained with

529   R^2=0.78-0.91 (P<0.01). 1 ppb increase in SO_2 likely increased N_{ccn} by 0.6×10^3 to 0.8

530    $\times 10^3$ cm^{-3} at SS from 0.2% to 1.0%. The increase in N_{ccn} with SO_2 may also reflect the

531   contribution from primary emissions. The intercepts of 2.2×10^3-2.7×10^3 cm^{-3} at

532   different SS were likely contributed by well-aged aerosols. The relationship may be

533   used as an estimation of N_{ccn} in marine atmospheres over China marginal seas, when

534   no measurements of CCN were available whereas ambient SO_2 can be estimated from

535   web-based satellite data.

4. Conclusions

Spatiotemporal variations in ambient N_{cn} and N_{ccn} were studied during a cruise campaign on DOY 110-135 over China marginal seas. The mean values of N_{cn} (8.1×10^3 cm^{-3}) and N_{ccn} (3.2 -3.9×10^3 cm^{-3}) at SS of 0.2%-1.0% were approximately one order of magnitude larger than those in remote clear marine atmospheres, indicating overwhelming contributions from non-sea-spray aerosols such as marine traffic emissions, the long-range continental transport and others.

Observed self-ship emission signals showed fresh marine traffic emissions can be important sources of N_{cn}, but a minor source of N_{ccn} in the marine atmosphere. The signals showed that 1 ppb increase in SO_2 corresponds to 1.4×10^4 cm^{-3} increase in N_{cn} and 30-170 cm^{-3} increase in N_{ccn} at SS=0.2-1.0%. Data analysis showed that marine traffic emissions largely increased N_{cn} over their heavily travelled sea zones in daytime.

In ambient marine air, the growth of marine traffic derived particles led to a decrease in estimated bulk kappa values at 0.4% possibly because some of these particles enriched in organics grew into CCN size. However, strong formation of ammonium salts led to aerosol aging, and significantly increased N_{ccn} at SS of 0.2-1.0% in comparison with those observed during the period poor in ammonium salt aerosols in $PM_{2.5}$ with P<0.01. The estimated bulk *Kappa* values from the daily average values varied from 0.46 to 0.55 at SS=0.4% in most of marine atmospheres, indicating inorganic ammonium aerosols may dominantly contribute to the N_{ccn} at SS of 0.4%. The particle number size distributions showed the high bulk *Kappa* values could be related to cloud-modified aerosols, which likely led to a large extent of degradation of organics and subsequently lost from the particle phase.

Humid marine ambient air led to NPF events rarely occurring therein. The dominant onshore winds occurred most of the measurement periods, and should carry primary aerosols and their aged products rather than secondarily formed aerosols to the

565 observational zone. During an occasion when offshore winds blew from the northwest

566 (Fig. S12), new particle signals transported from the continent can be clearly observed.

567 However, NPF in the marine atmosphere was too weak to be important. The transported

568 new particles from the continent yielded the maximal increase in N_{ccn} by 92% at SS of

569 0.4% and 150% at SS of 1.0%. However, consistent with those reported in literature,

570 the estimated *kappa* values largely decreased from 0.4 to 0.1-0.2 at SS=0.4% during

571 most time of the continent-transported NPF event because of the *kappa* value of organic

572 condensation vapor as low as 0.1.

573

582

583 **References**

584 Andreae, M. O., and Rosenfeld, D.: Aerosol-cloud-precipitation interactions. Part 1. The

585 nature and sources of cloud-active aerosols, Earth-Sci. Rev., 89, 13-41,

586 10.1016/j.earscirev.2008.03.001, 2008.

587 Blot, R., Clarke, A. D., Freitag, S., Kapustin, V., Howell, S. G., Jensen, J. B., Shank, L.

588 M., McNaughton, C. S., and Brekhovskikh, V.: Ultrafine sea spray aerosol over the

589 southeastern Pacific: open-ocean contributions to marine boundary layer CCN,

590 Atmos. Chem. Phys., 13, 7263-7278, 10.5194/acp-13-7263-2013, 2013.

591 Bougiatioti, A., Fountoukis, C., Kalivitis, N., Pandis, S. N., Nenes, A., and Mihalopoulos,

592 N.: Cloud condensation nuclei measurements in the eastern Mediterranean marine

593 boundary layer: CCN closure and droplet growth kinetics, Atmos. Chem.

Phys.Discuss., 9, 10303-10336, 10.5194/acpd-9-10303-2009, 2009.

Brooks, S. D., and Thornton, D. C. O.: Marine Aerosols and Clouds, Annu. Rev. Mar. Sci., 10, 289-313, 10.1146/annurev-marine-121916-063148, 2018.

Cai, M. F., Tan, H. B., Chan, C. K., Mochida, M., Hatakeyama, S., Kondo, Y., Schurman, M. I., Xu, H. B., Li, F., Shimada, K., Li, L., Deng, Y. G., Yai, H., Matsuki, A., Qin, Y. M., and Zhao, J.: Comparison of Aerosol Hygroscopcity, Volatility, and Chemical Composition between a Suburban Site in the Pearl River Delta Region and a Marine Site in Okinawa, Aerosol. Air. Qual. Res., 17, 3194-3208, 10.4209/aaqr.2017.01.0020, 2017.

Charlson, R. J., Lovelock, J. E., Andreae, M. O., and Warren, S. G.: Oceanic phytoplankton atmospheric sulpher cloud albedo and climate, Nature, 326, 655-661, 1987.

Chen, D. S., Wang, X. T., Li, Y., Lang, J. L., Zhou, Y., Guo, X. R., and Zhao, Y. H.: High-spatiotemporal-resolution ship emission inventory of China based on AIS data in 2014, Sci. Total Environ., 609, 776-787, 10.1016/j.scitotenv.2017.07.051, 2017.

Cheung, H. C., Chou, C. C.-K., Lee, C. S. L., Kuo, W.-C., and Chang, S.-C.: Hygroscopic properties and cloud condensation nuclei activity of atmospheric aerosols under the influences of Asian continental outflow and new particle formation at a coastal site in eastern Asia, Atmos. Chem. Phys., 20, 5911–5922, https://doi.org/10.5194/acp-20-5911-2020, 2020.

Clarke, A. D., Owens, S. R., and Zhou, J. C.: An ultrafine sea-salt flux from breaking waves: Implications for cloud condensation nuclei in the remote marine atmosphere, J. Geophys. Res.-Atmos., 111, Artn D06202,10.1029/2005jd006565, 2006.

Crippa, M., Canonaco, F., Lanz, V. A., Aijala, M., Allan, J. D., Carbone, S., Capes, G., Ceburnis, D., Dall'Osto, M., Day, D. A., DeCarlo, P. F., Ehn, M., Eriksson, A., Freney, E., Hildebrandt Ruiz, L., Hillamo, R., Jimenez, J. L., Junninen, H., Kiendler-Scharr, A., Kortelainen, A. M., Kulmala, M., Laaksonen, A., Mensah, A., Mohr, C., Nemitz, E., O'Dowd, C., Ovadnevaite, J., Pandis, S. N., Petaja, T., Poulain, L., Saarikoski, S., Sellegri, K., Swietlicki, E., Tiitta, P., Worsnop, D. R., Baltensperger, U., and Prevot, A. S. H.: Organic aerosol components derived from 25 AMS data sets across Europe

using a consistent ME-2 based source apportionment approach, Atmos. Chem. Phys., 14, 6159-6176, 10.5194/acp-14-6159-2014, 2014.

Dal Maso, M., Kulmala, M., Riipinen, I., Wagner, R., Hussein, T., Aalto, P. P., and Lehtinen, K. E. J.: Formation and growth of fresh atmospheric aerosols: eight years of aerosol size distribution data from SMEAR II, Hyytiala, Finland, Boreal Environ. Res., 10, 323-336, 2005.

Dal Maso, M., Gao, J., Jarvinen, A., Li, H., Luo, D. T., Janka, K., and Ronkko, T.: Improving Urban Air Quality Measurements by a Diffusion Charger Based Electrical Particle Sensors - A Field Study in Beijing, China, Aerosol. Air. Qual. Res., 16, 3001-3011, 10.4209/aaqr.2015.09.0546, 2016.

Decesari, S., Finessi, E., Rinaldi, M., Paglione, M., Fuzzi, S., Stephanou, E. G., Tziaras, T., Spyros, A., Ceburnis, D., O'Dowd, C., Dall'Osto, M., Harrison, R. M., Allan, J., Coe, H., and Facchini, M. C.: Primary and secondary marine organic aerosols over the North Atlantic Ocean during the MAP experiment, J. Geophys. Res.-Atmos., 116, Artn D22210,10.1029/2011jd016204, 2011.

Ding, X., Qi, J. H., and Meng, X. B.: Characteristics and sources of organic carbon in coastal and marine atmospheric particulates over East China, Atmos. Res., 228, 281-291, 10.1016/j.atmosres.2019.06.015, 2019.

Dusek, U., Frank, G. P., Hildebrandt, L., Curtius, J., Schneider, J., Walter, S., Chand, D., Drewnick, F., Hings, S., Jung, D., Borrmann, S., and Andreae, M. O.: Size matters more than chemistry for cloud-nucleating ability of aerosol particles, Science, 312, 1375-1378, 10.1126/science.1125261, 2006.

Feng, J. L., Guo, Z. G., Zhang, T. R., Yao, X. H., Chan, C. K., and Fang, M.: Source and formation of secondary particulate matter in PM2.5 in Asian continental outflow, J. Geophys. Res.-Atmos., 117, Artn D03302,10.1029/2011jd016400, 2012.

Feng, L., Shen, H., Zhu, Y., Gao, H., and Yao, X.: Insight into Generation and Evolution of Sea-Salt Aerosols from Field Measurements in Diversified Marine and Coastal Atmospheres, Sci. Rep., 7, 41260, 10.1038/srep41260, 2017.

Feng, T., Li, G. H., Cao, J. J., Bei, N. F., Shen, Z. X., Zhou, W. J., Liu, S. X., Zhang, T., Wang, Y. C., Huang, R. J., Tie, X. X., and Molina, L. T.: Simulations of organic

aerosol concentrations during springtime in the Guanzhong Basin, China, Atmos. Chem. Phys., 16, 10045-10061, 10.5194/acp-16-10045-2016, 2016.

Fossum, K. N., Ovadnevaite, J., Ceburnis, D., Dall'Osto, M., Marullo, S., Bellacicco, M., Simo, R., Liu, D. T., Flynn, M., Zuend, A., and O'Dowd, C.: Summertime Primary and Secondary Contributions to Southern Ocean Cloud Condensation Nuclei, Sci. Rep., 8, Artn 13844,10.1038/S41598-018-32047-4, 2018.

Fu, X. G., Wang, M., Zeng, S. Q., Feng, X. L., Wang, D., and Song, C. Y.: Continental weathering and palaeoclimatic changes through the onset of the Early Toarcian oceanic anoxic event in the Qiangtang Basin, eastern Tethys, Palaeogeogr. Palaeocl., 487, 241-250, 10.1016/j.palaeo.2017.09.005, 2017.

Gunthe, S. S., Rose, D., Su, H., Garland, R. M., Achtert, P., Nowak, A., Wiedensohler, A., Kuwata, M., Takegawa, N., Kondo, Y., Hu, M., Shao, M., Zhu, T., Andreae, M. O., and Pöschl, U.: Cloud condensation nuclei (CCN) from fresh and aged air pollution in the megacity region of Beijing, Atmos. Chem. Phys., 11, 11023-11039, 10.5194/acp-11-11023-2011, 2011.

Guo, L., Chen, Y., Wang, F., Meng, X., Xu, Z., and Zhuang, G.: Effects of Asian dust on the atmospheric input of trace elements to the East China Sea, Mar. Chem., 163, 19-27, 10.1016/j.marchem.2014.04.003, 2014.

Guo, T., Li, K., Zhu, Y., Gao, H., and Yao, X.: Concentration and size distribution of particulate oxalate in marine and coastal atmospheres – Implication for the increased importance of oxalate in nanometer atmospheric particles, Atmos. Environ., 142, 19-31, 10.1016/j.atmosenv.2016.07.026, 2016.

Hoppel W. A., F. G. M., and Larson R. E.: Effect of non-precipitating clouds on the aerosol size distribution, Geophys. Res. Lett., 13, 125-128, 1986.

Huebert, B. J., Bates, T., Russell, P. B., Shi, G. Y., Kim, Y. J., Kawamura, K., Carmichael, G., and Nakajima, T.: An overview of ACE-Asia: Strategies for quantifying the relationships between Asian aerosols and their climatic impacts, J. Geophys. Res.-Atmos., 108, Artn 8633,10.1029/2003jd003550, 2003.

Hung, H. M., Lu, W. J., Chen, W. N., Chang, C. C., Chou, C. C. K., and Lin, P. H.: Enhancement of the hygroscopicity parameter kappa of rural aerosols in northern

Taiwan by anthropogenic emissions, Atmos. Environ., 84, 78-87, 10.1016/j.atmosenv.2013.11.032, 2014.

Kerminen, V. M., Chen, X. M., Vakkari, V., Petaja, T., Kulmala, M., and Bianchi, F.: Atmospheric new particle formation and growth: review of field observations, Environ. Res. Lett., 13, Artn 103003,10.1088/1748-9326/Aadf3c, 2018.

Kulmala, M., Vehkamaki, H., Petaja, T., Dal Maso, M., Lauri, A., Kerminen, V. M., Birmili, W., and McMurry, P. H.: Formation and growth rates of ultrafine atmospheric particles: a review of observations, J. Aer. Sci., 35, 143-176, 10.1016/j.jaerosci.2003.10.003, 2004.

Langley, L., Leaitch, W. R., Lohmann, U., Shantz, N. C., and Worsnop, D. R.: Contributions from DMS and ship emissions to CCN observed over the summertime North Pacific, Atmos. Chem. Phys., 10, 1287-1314, DOI 10.5194/acp-10-1287-2010, 2010.

Leng, C., Cheng, T., Chen, J., Zhang, R., Tao, J., Huang, G., Zha, S., Zhang, M., Fang, W., Li, X., and Li, L.: Measurements of surface cloud condensation nuclei and aerosol activity in downtown Shanghai, Atmos. Environ., 69, 354-361, 10.1016/j.atmosenv.2012.12.021, 2013.

Li, K., Zhu, Y., Gao, H., and Yao, X.: A comparative study of cloud condensation nuclei measured between non-heating and heating periods at a suburb site of Qingdao in the North China, Atmos. Environ., 112, 40-53, 10.1016/j.atmosenv.2015.04.024, 2015.

Li, M., Liu, H., Geng, G., Hong, C., Liu, F., Song, Y., Tong, D., Zheng, B., Cui, H., Man, H., Zhang, Q., and He, K.: Anthropogenic emission inventories in China: a review, Natl. Sci. Rev., 4, 834-866, 10.1093/nsr/nwx150, 2017.

Lin, Y. C., Chen, J. P., Ho, T. Y., and Tsai, I. C.: Atmospheric iron deposition in the northwestern Pacific Ocean and its adjacent marginal seas: The importance of coal burning, Global. Biogeochem. Cy., 29, 138-159, 10.1002/2013GB004795, 2015.

Liu, F., Zhang, Q., A., R. J. v. d., Zheng, B., Tong, D., Yan, L., Zheng, Y., and He, K.: Recent reduction in NO x emissions over China: synthesis of satellite observations and emission inventories, Environ. Res. Lett., 11, 114002, 2016.

Ma, N., Zhao, C. S., Tao, J. C., Wu, Z. J., Kecorius, S., Wang, Z. B., Gross, J., Liu, H.

714   J., Bian, Y. X., Kuang, Y., Teich, M., Spindler, G., Muller, K., van Pinxteren, D.,

715   Herrmann, H., Hu, M., and Wiedensohler, A.: Variation of CCN activity during new

716   particle formation events in the North China Plain, Atmos. Chem. Phys., 16, 8593-

717   8607, 10.5194/acp-16-8593-2016, 2016.

718 Mochida, M., Nishita-Hara, C., Kitamori, Y., Aggarwal, S. G., Kawamura, K., Miura,

719   K., and Takami, A.: Size-segregated measurements of cloud condensation nucleus

720   activity and hygroscopic growth for aerosols at Cape Hedo, Japan, in spring 2008, J.

721   Geophys. Res., 115, 10.1029/2009jd013216, 2010.

722 Nair, V. S., Nair, J. V., Kompalli, S. K., Gogoi, M. M., and Babu, S. S.: Cloud

723   Condensation Nuclei properties of South Asian outflow over the northern Indian

724   Ocean during winter, Atmos. Chem. Phys.Discuss., 10.5194/acp-2019-828, 2019.

725 O'Dowd, C., Ceburnis, D., Ovadnevaite, J., Vaishya, A., Rinaldi, M., and Facchini, M.

726   C.: Do anthropogenic, continental or coastal aerosol sources impact on a marine

727   aerosol signature at Mace Head?, Atmos. Chem. Phys., 14, 10687-10704,

728   10.5194/acp-14-10687-2014, 2014.

729 O'Dowd, C. D., Smith, M. H., Consterdine, I. E., and Lowe, J. A.: Marine aerosol, sea-

730   salt, and the marine sulphur cycle: A short review, Atmos. Environ., 31, 73-80, Doi

731   10.1016/S1352-2310(96)00106-9, 1997.

732 O'Dowd, C. D., Facchini, M. C., Cavalli, F., Ceburnis, D., Mircea, M., Decesari, S.,

733   Fuzzi, S., Yoon, Y. J., and Putaud, J. P.: Biogenically driven organic contribution to

734   marine aerosol, Nature, 431, 676-680, 10.1038/nature02959, 2004.

735 Park, M., Yum, S. S., Kim, N., Cha, J. W., Shin, B., and Ryoo, S.-B.: Characterization

736   of submicron aerosols and CCN over the Yellow Sea measured onboard the Gisang

737   1 research vessel using the positive matrix factorization analysis method, Atmos.

738   Res., 214, 430-441, 10.1016/j.atmosres.2018.08.015, 2018.

739 Petters, M. D., and Kreidenweis, S. M.: A single parameter representation of hygroscopic

740   growth and cloud condensation nucleus activity, Atmos. Chem. Phys., 7, 1961-1971,

741   DOI 10.5194/acp-7-1961-2007, 2007.

742 Phillips, B. N., Royalty, T. M., Dawson, K. W., Reed, R., Petters, M. D., and Meskhidze,

743   N.: Hygroscopicity- and Size-Resolved Measurements of Submicron Aerosol on the

East Coast of the United States, J. Geophys. Res.-Atmos., 123, 1826-1839, 10.1002/2017JD027702, 2018.

Pöschl, U., Rose, D., & Andreae, M. O. (2009). Climatologies of Cloud-related Aerosols. Part 2: Particle Hygroscopicity and Cloud Condensation Nucleus Activity. In J. Heintzenberg, & R. J. Charlson (Eds.), Clouds in the Perturbed Climate System: Their Relationship to Energy Balance, Atmospheric Dynamics, and Precipitation (pp. 58-72). Cambridge: MIT Press.

Quinn, P. K., and Bates, T. S.: The case against climate regulation via oceanic phytoplankton sulphur emissions, Nature, 480, 51-56, 10.1038/nature10580, 2011.

Quinn, P. K., Collins, D. B., Grassian, V. H., Prather, K. A., and Bates, T. S.: Chemistry and Related Properties of Freshly Emitted Sea Spray Aerosol, Chem. Rev., 115, 4383-4399, 10.1021/cr500713g, 2015.

Ramana, M. V., and Devi, A.: CCN concentrations and BC warming influenced by maritime ship emitted aerosol plumes over southern Bay of Bengal, Sci. Rep., 6, 30416, 10.1038/srep30416, 2016.

Rose, D., Gunthe, S. S., Mikhailov, E., Frank, G. P., Dusek, U., Andreae, M. O., and Pöschl, U.: Calibration and measurement uncertainties of a continuous-flow cloud condensation nuclei counter (DMT-CCNC): CCN activation of ammonium sulfate and sodium chloride aerosol particles in theory and experiment, Atmos. Chem. Phys., 8, 1153–1179, https://doi.org/10.5194/acp-8-1153-2008, 2008.

Rose, D., Nowak, A., Achtert, P., Wiedensohler, A., Hu, M., Shao, M., Zhang, Y., Andreae, M. O., and Pöschl, U.: Cloud condensation nuclei in polluted air and biomass burning smoke near the mega-city Guangzhou, China - Part 1: Size-resolved measurements and implications for the modeling of aerosol particle hygroscopicity and CCN activity, Atmos. Chem. Phys., 10, 3365-3383, DOI 10.5194/acp-10-3365-2010, 2010.

Rose, D., Gunthe, S. S., Su, H., Garland, R. M., Yang, H., Berghof, M., Cheng, Y. F., Wehner, B., Achtert, P., Nowak, A., Wiedensohler, A., Takegawa, N., Kondo, Y., Hu, M., Zhang, Y., Andreae, M. O., and Pöschl, U.: Cloud condensation nuclei in polluted air and biomass burning smoke near the mega-city Guangzhou, China – Part 2: Size-

774   resolved aerosol chemical composition, diurnal cycles, and externally mixed weakly

775   CCN-active soot particles, Atmos. Chem. Phys., 11, 2817-2836, 10.5194/acp-11-

776   2817-2011, 2011.

777 Rosenfeld, D., Zhu, Y. N., Wang, M. H., Zheng, Y. T., Goren, T., and Yu, S. C.: Aerosol-

778   driven droplet concentrations dominate coverage and water of oceanic low-level

779   clouds, Science, 363, 10.1126/science.aav0566, 2019.

780 Royalty, T. M., Phillips, B. N., Dawson, K. W., Reed, R., Meskhidze, N., and Petters, M.

781   D.: Aerosol Properties Observed in the Subtropical North Pacific Boundary Layer, J.

782   Geophys. Res.-Atmos., 122, 9990-10012, 10.1002/2017JD026897, 2017.

783 Ruehl, C. R., Chuang, P. Y., and Nenes, A.: Distinct CCN activation kinetics above the

784   marine boundary layer along the California coast, Geophys. Res. Lett., 36, L15814,

785   10.1029/2009gl038839, 2009.

786 Saliba, G., Chen, C. L., Lewis, S., Russell, L. M., Rivellini, L. H., Lee, A. K. Y., Quinn,

787   P. K., Bates, T. S., Haentjens, N., Boss, E. S., Karp-Boss, L., Baetge, N., Carlson, C.

788   A., and Behrenfeld, M. J.: Factors driving the seasonal and hourly variability of sea-

789   spray aerosol number in the North Atlantic, Proc. Natl. Acad. Sci. U.S.A., 116,

790   20309-20314, 10.1073/pnas.1907574116, 2019.

791 Sato, Y., and Suzuki, K.: How do aerosols affect cloudiness? Science, 363, 580-581,

792   10.1126/science.aaw3720, 2019.

793 Singla, V., Mukherjee, S., Safai, P. D., Meena, G. S., Dani, K. K., and Pandithurai, G.:

794   Role of organic aerosols in CCN activation and closure over a rural background site

795   in   Western   Ghats,   India,   Atmos.   Environ.,   158,   148-159,

796   10.1016/j.atmosenv.2017.03.037, 2017.

797 Song, J. W., Zhao, Y., Zhang, Y. Y., Fu, P. Q., Zheng, L. S., Yuan, Q., Wang, S., Huang,

798   X. F., Xu, W. H., Cao, Z. X., Gromov, S., and Lai, S. C.: Influence of biomass burning

799   on atmospheric aerosols over the western South China Sea: Insights from ions,

800   carbonaceous fractions and stable carbon isotope ratios, Environ. Pollut., 242, 1800-

801   1809, 10.1016/j.envpol.2018.07.088, 2018.

802 Ueda, S., Miura, K., Kawata, R., Furutani, H., Uematsu, M., Omori, Y., and Tanimoto,

803   H.: Number-size distribution of aerosol particles and new particle formation events

in tropical and subtropical Pacific Oceans, Atmos. Environ., 142, 324-339, 10.1016/j.atmosenv.2016.07.055, 2016.

Wang, J., Shen, Y., Li, K., Gao, Y., Gao, H., and Yao, X.: Nucleation-mode particle pool and large increases in Ncn and Nccn observed over the northwestern Pacific Ocean in the spring of 2014, Atmos. Chem. Phys., 19, 8845-8861, 10.5194/acp-19-8845-2019, 2019.

Wang, Z. J., Du, L. B., Li, X. X., Meng, X. Q., Chen, C., Qu, J. L., Wang, X. F., Liu, X. T., and Kabanov, V. V.: Observations of marine aerosol by a shipborne multiwavelength lidar over the Yellow Sea of China, Proc. SPIE 9262, Lidar Remote Sensing for Environmental Monitoring XIV, 926218 10.1117/12.2070297, 2014.

Wu, Z. J., Zheng, J., Shang, D. J., Du, Z. F., Wu, Y. S., Zeng, L. M., Wiedensohler, A., and Hu, M.: Particle hygroscopicity and its link to chemical composition in the urban atmosphere of Beijing, China, during summertime, Atmos. Chem. Phys., 16, 1123-1138, 10.5194/acp-16-1123-2016, 2016.

Yamashita, K., Murakami, M., Hashimoto, A., and Tajiri, T.: CCN Ability of Asian Mineral Dust Particles and Their Effects on Cloud Droplet Formation, J. Meteor. Soc. Japan, 89, 581-587, 10.2151/jmsj.2011-512, 2011.

Yao, X. H., Lau, N. T., Fang, M., and Chan, C. K.: Real-time observation of the transformation of ultrafine atmospheric particle modes, Aerosol. Sci. Tech., 39, 831-841, 10.1080/02786820500295248, 2005.

Yao, X. H., Lau, N. T., Chan, C. K., and Fang, M.: Size distributions and condensation growth of submicron particles in on-road vehicle plumes in Hong Kong, Atmos. Environ., 41, 3328-3338, 10.1016/j.atmosenv.2006.12.044, 2007.

Yao, X. H., Choi, M. Y., Lau, N. T., Lau, A. P. S., Chan, C. K., and Fang, M.: Growth and Shrinkage of New Particles in the Atmosphere in Hong Kong, Aerosol. Sci. Tech., 44, 639-650, Pii 924397031,10.1080/02786826.2010.482576, 2010.

Yu, F., and Luo, G.: Simulation of particle size distribution with a global aerosol model: contribution of nucleation to aerosol and CCN number concentrations, Atmos. Chem. Phys., 9, 7691-7710, DOI 10.5194/acp-9-7691-2009, 2009.

Zhu, Y. J., Li, K., Shen, Y. J., Gao, Y., Liu, X. H., Yu, Y., Gao, H. W., and Yao, X. H.:

834   New particle formation in the marine atmosphere during seven cruise campaigns,

835   Atmos. Chem. Phys., 19, 89-113, 10.5194/acp-19-89-2019, 2019.

836 Zimmerman, N., Jeong, C.-H., Wang, J. M., Ramos, M., Wallace, J. S., and Evans, G.

837   J.: A source-independent empirical correction procedure for the fast mobility and

838   engine   exhaust   particle   sizers,   Atmos.   Environ.,   100,   178-184,
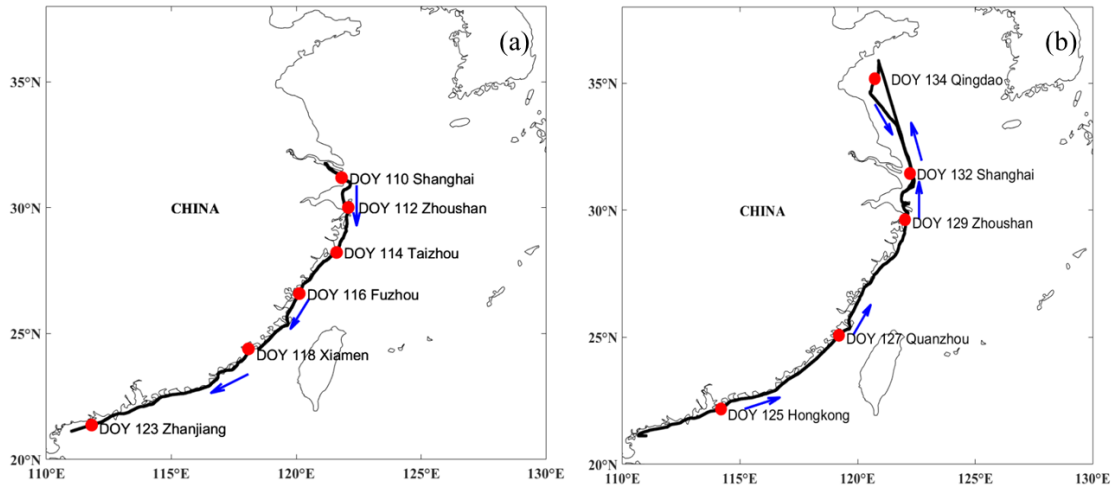
839   10.1016/j.atmosenv.2014.10.054, 2015.

840

Fig 1 The ship track during the campaign of 2018, and the blue arrows represented the sailing direction, with southward track (a) and northward track (b).
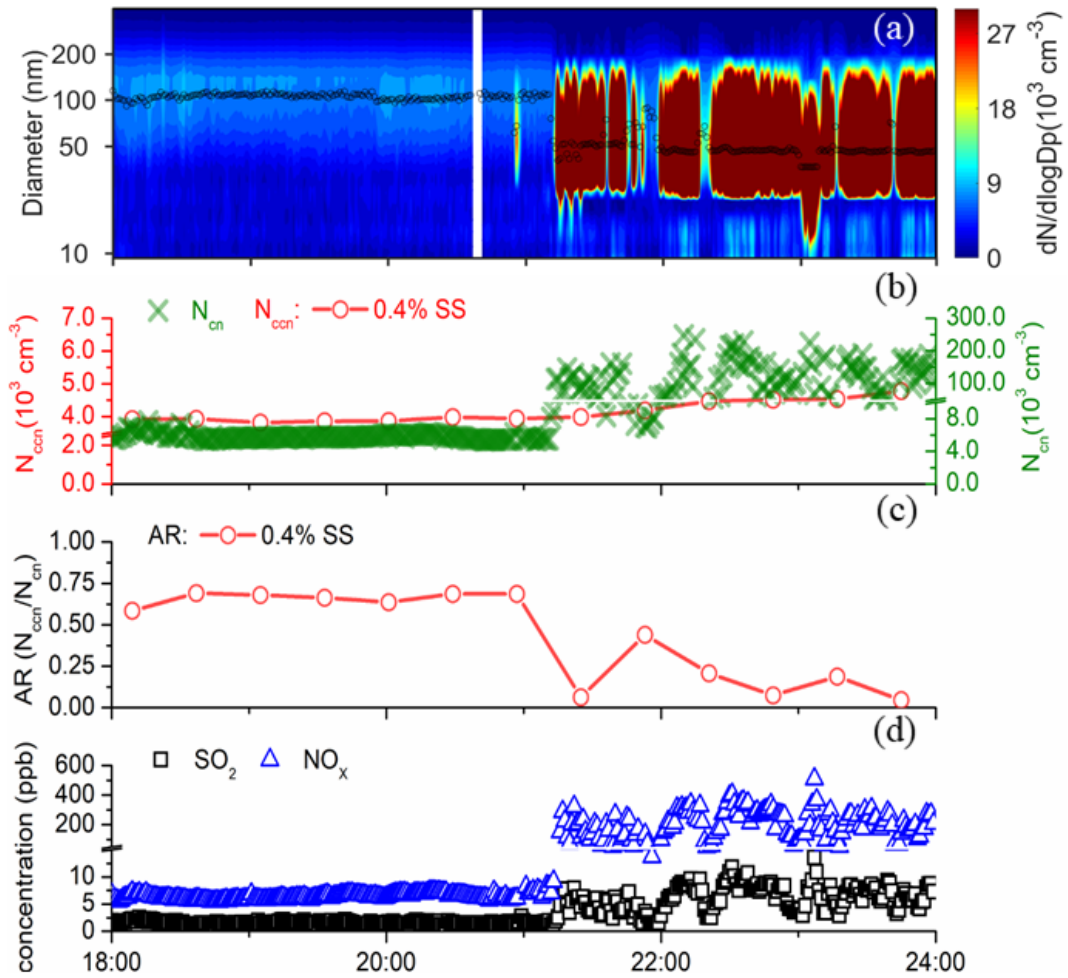
Fig 2 Contour plot of particle number size distribution with the median mobility mode diameter shown in black hollow circles (a), time series of minutely N_{cn} and half-hourly N_{ccn} at SS=0.4% (b), half-hourly AR values at SS=0.4% (c), SO_2 and NO_x at nighttime on DOY 115.
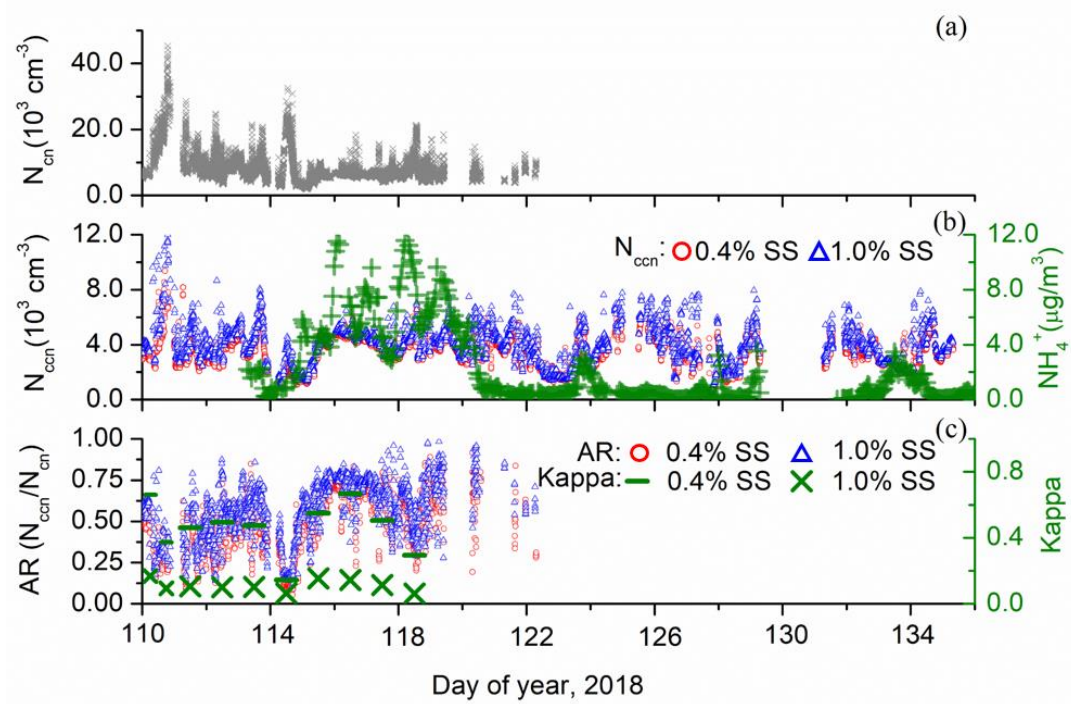
Fig 3 Time series of minutely N_{cn} from DOY 110 to 122 (a), minutely N_{ccn} at SS of 0.4% and 1.0% during DOY 110-135 and hourly NH_4^+ during DOY 113-135 (b), and minutely AR at SS of 0.4% and 1.0% during DOY 110-122 and daily *Kappa* values at SS of 0.4% and 1.0% from DOY 110 to 118 due to data availability (c). Please note that for Fig. 3c, most *Kappa* values were based on daily scale, except on DOY 110, during which two *Kappa* values were calculated from 00:00-06:00 and 08:00-21:00, respectively.
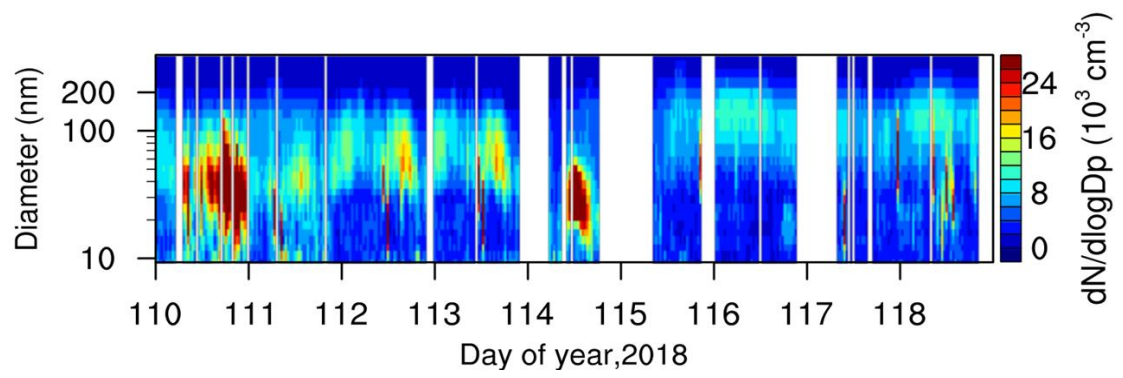
Fig 4 Contour plot of particle number size distribution on DOY 110-118 with self-ship emission signals removed.
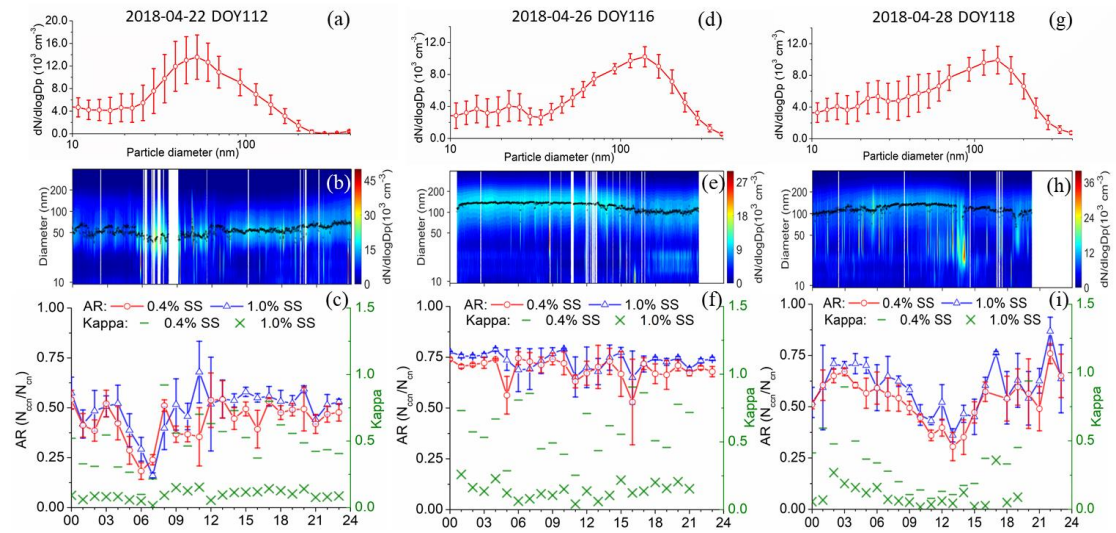
Fig 5 Daily average (top row) and contour plot (middle row) of particle number size distributions, and time series of hourly averaged AR at SS of 0.4% and 1.0% and *Kappa* value on DOY112, DOY116 and DOY118. The bars represent the standard deviation with mean indicated by the hollow circles.
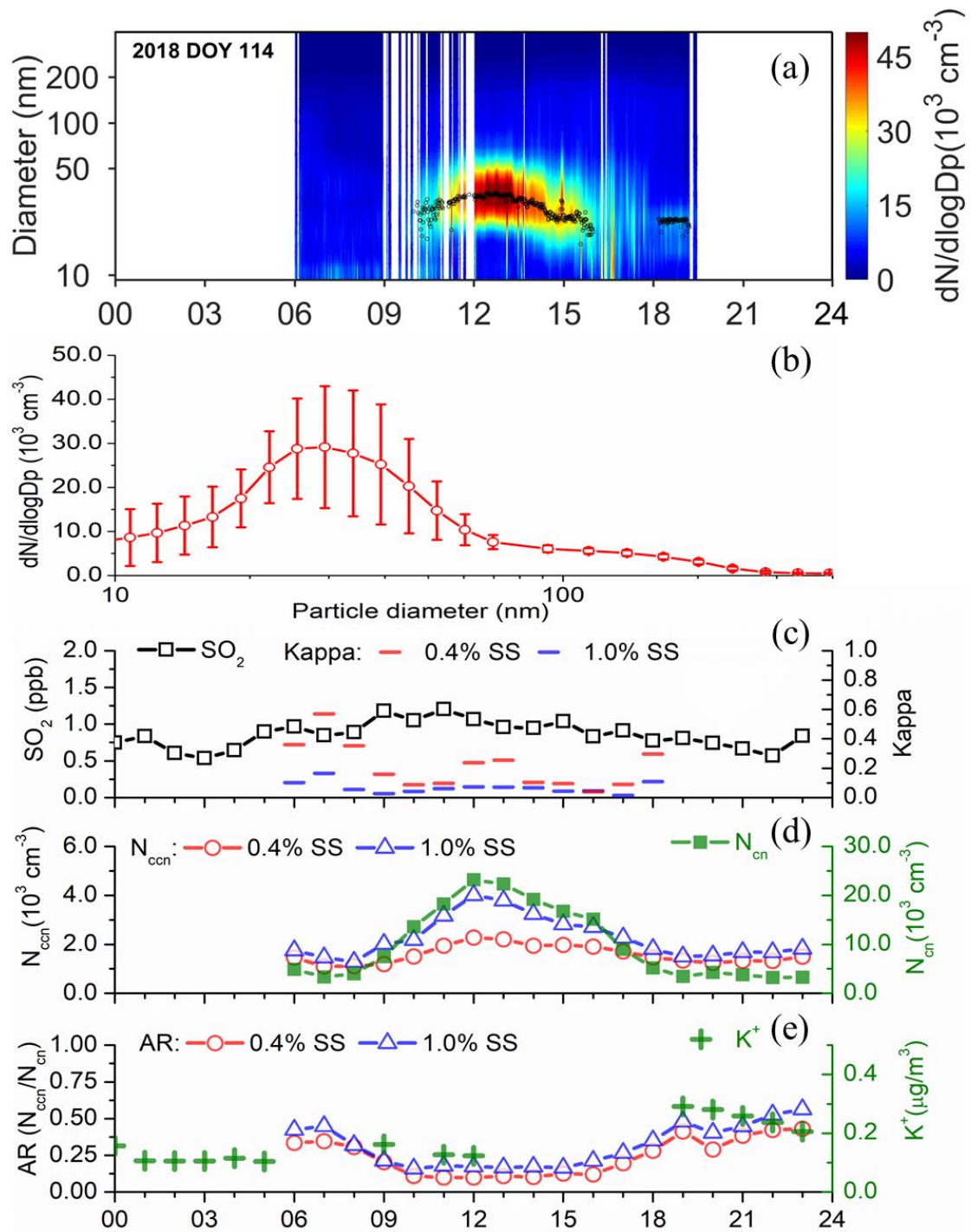
Fig 6 Contour plot of particle number size distributions for the day of DOY 114 2018 (a), the size distributions of particle number concentration during 10:00 -18:00 LT DOY 114 2018 (b), time series of hourly averaged SO_2 and *Kappa* values at SS of 0.4% and 1.0% (c), N_{ccn} at SS of 0.4% and 1.0% (d), and AR values at SS of 0.4% and 1.0% and K^+ (e) for the day of DOY 114 2018.
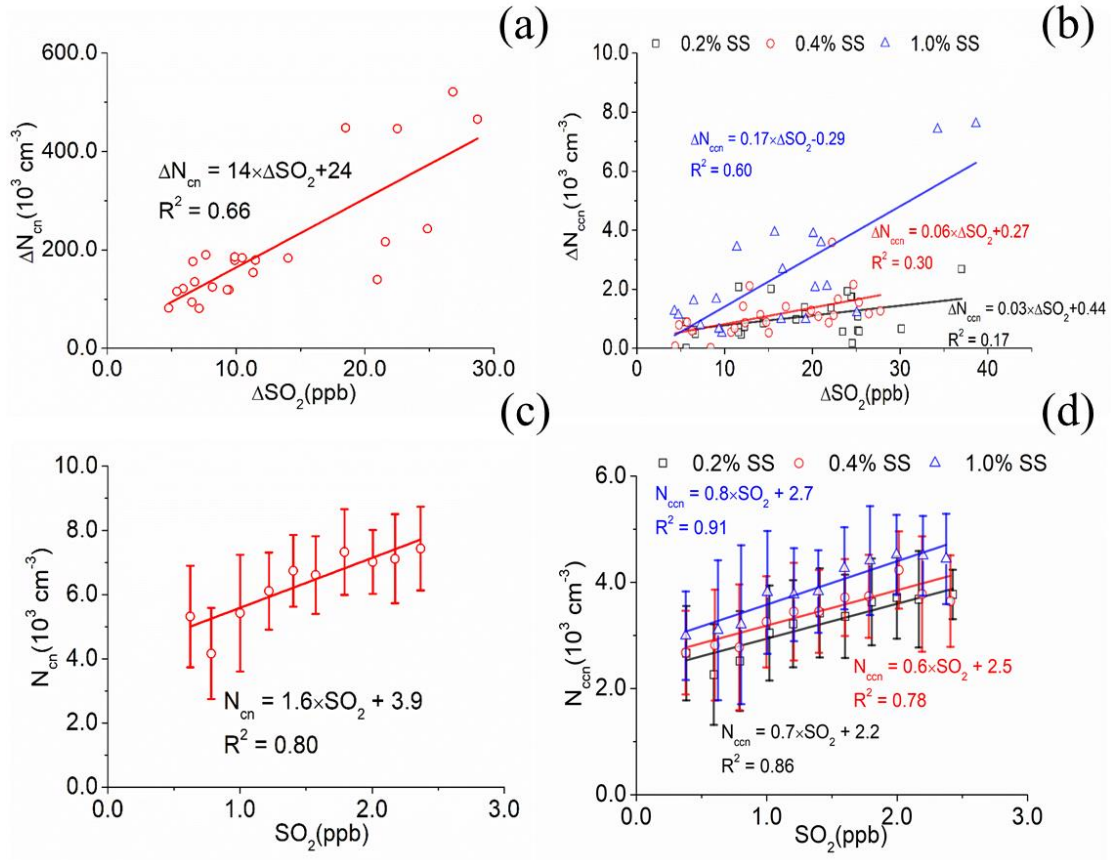
Fig 7 Correlations of hourly averaged N_{cn} and N_{ccn} with SO_2 at SS of 0.2%, 0.4% and 1.0%. For Fig. 7a,b, $\triangle N_{cn}$, $\triangle N_{ccn}$ and $\triangle SO_2$ reflects the impact from self-ship emission after the removal of ambient concentration. For Fig. 7c,d each bar indicates standard deviation with mean value marked as the hollow circles (or triangles, squares), and the interval of SO_2 is 0.2 ppb for each bar.

Table 1. N_{cn} and N_{ccn}, AR and SO_2 mixing ratios on DOY 110-135, 2018 over China marginal seas. Please note that Ncn and AR are from 110-122, 2018.

Variables	Supersaturation (SS)	Ranges	Mean ± standard deviation
N_{cn} ($\times10^3$ cm^{-3})		2.0-45	8.1±4.4
	SS=0.2%	0.4-8.8	3.2±1.1
	SS=0.4%	0.5-9.4	3.4±1.1
N_{ccn} ($\times10^3$ cm^{-3})	SS=0.6%	0.5-8.6	3.6±1.2
	SS=0.8%	0.5-11	3.8±1.2
	SS=1.0%	0.6-12	3.9±1.4
	SS=0.2%	0.06-0.89	0.49±0.17
	SS=0.4%	0.06-0.92	0.51±0.17
AR	SS=0.6%	0.10-0.94	0.54±0.17
	SS=0.8%	0.08-0.95	0.56±0.17
	SS=1.0%	0.11-0.98	0.57±0.17
SO_2 (ppb)		0.25-9.7	1.7±1.1